Available online at www.sciencedirect.com

ScienceDirect

Procedia Technology 17 (2014) 194 – 201

Procedia Technology

Conference on Electronics, Telecommunications and Computers – CETC 2013

Characterization of Combustion Chemiluminescence: an Image Processing Approach

Teodoro Trindade[a,1], Artur Ferreira[a], Edgar Fernandes[b]

[a]*Instituto Superior de Engenharia de Lisboa, Rua Conselheiro Emidio Navarro, n. 1, 1959-007 Lisboa, Portugal*
[b]*Instituto Superior Técnico, Av. Rovisco Pais, n. 1, 1049-001 Lisboa, Portugal*

Abstract

The applicability of image data processing to estimate the spatial distribution of Air/Fuel ratio at the flame front on gas combustion systems are presented and discussed. The objective is to devise a procedure capable of converting a single RGB image data, obtained by conventional CCD cameras, into a reliable sensing on local combustion state for practical application on atmospheric flames of premixed methane and propane gases. In this context, this paper proposes a fast and innovative image processing methodology. An image processing algorithm based on the camera sensor transfer function, a lookup calibration table, and sparse matrices operations is proposed. The optimized version of our image processing algorithm is able to process high resolution images at rates as high as 0.6 Mpixel/s on a standard personal computer (3.5 GHz clock frequency). As a result, color RGB images are converted into quasi real-time detectors of local combustion state for practical flames of CH_4 and C_3H_8 gases. It has been experimentally observed that camera blue and green channels mimic the flame CH^* and C_2^* chemiluminescence emissions, revealing a wide applicability on ϕ detection (Air/Fuel ratio), roughly ranging between 0.8 and 1.4.

Peer-review under responsibility of ISEL – Instituto Superior de Engenharia de Lisboa, Lisbon, PORTUGAL.
Keywords: flame chemiluminescence, gas premixed combustion, equivalence ratio sensor, intensity-response model, image processing, RGB images, sparse matrix

1. Introduction

A rational use of fuel on gas combustion processes demands for efficient control devices with fast time response, where pollutant emissions, gas temperature, or soot particle concentration are the typical control set-points. In order to achieve a desired performance, sensors are critical elements where type and adequate location inside the combustion system are crucial. Preferably, a control scheme based on monitoring the flame front has an advantage of low time constant when compared with others intrusive diagnostic techniques such as thermocouples, chemical sensors, etc. Despite the existence of a wide range of non-intrusive diagnostic techniques able to extract useful information

* Corresponding author. Instituto Superior de Engenharia de Lisboa, Rua Conselheiro Emidio Navarro, n.1, 1959-007 Lisboa, Portugal.
E-mail address: teodoro@deq.isel.ipl.pt

Peer-review under responsibility of ISEL – Instituto Superior de Engenharia de Lisboa, Lisbon, PORTUGAL.
doi:10.1016/j.protcy.2014.10.228

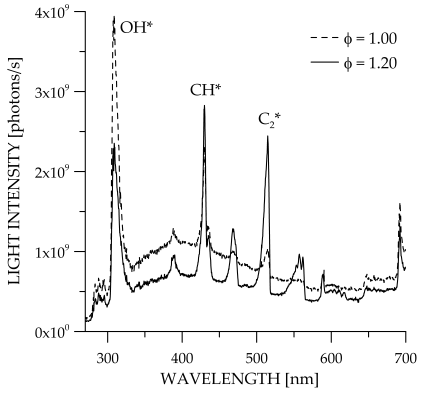

Fig. 1. Light emission spectrum in near-ultraviolet/visible region of premixed CH_4/air flames (1.75 kW). Stoichiometric ϕ=1.0 (dashed line); fuel rich ϕ=1.2 (solid line).

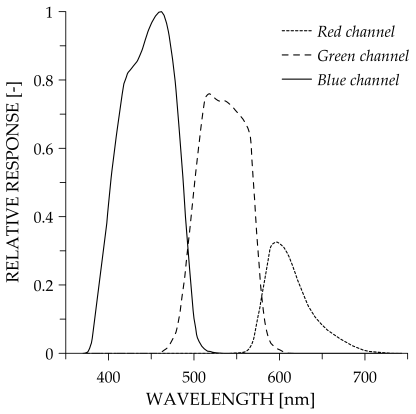

Fig. 2. Spectral sensitivity curves $S_i(\lambda)$ of each R, G, and B sensor channels, obtained experimentally for the overall camera assembly (JAI CV-M9GE).

from a flame [1,2], many of these sophisticated sensors have severe limitations regarding their practical use in harsh environments due to lack of ruggedness, extreme optical complexities, and high cost, among other aspects. Although, a simple non-intrusive optical technique that exploits the radiation spontaneously emitted by flames, termed as *chemiluminescence*, has been widely quoted for combustion diagnostics [3–6]. Since chemiluminescence provides inside information on the process of kinetic chemistry, changes in the burning conditions have an instantaneous effect on emissions and thus in the light that reaches the sensor. Chemiluminescence of excited radicals such as CH^* and C_2^* formed within the reaction zone, constitutes a *signature* of the burning conditions [4,7]. These two types of chemical species are the most abundant excited radicals produced within the flame front, emitting as narrow bands in the visible region of the electromagnetic spectrum (Figure 1), centered around the wavelengths 430 nm (CH^*) and 515 nm (C_2^*). The relative densities of these emitters are the key responsibles for the hydrocarbon flame color, captured by photo-sensors.

1.1. Flame Images

Imaging devices based on digital *charge coupled device* (CCD) array constitute a recent generation of photo-sensors with potential applications on combustion monitoring, control, and burner's engineering project. Digital cameras act as an array of sensors that are sensitive to light. The output signal of each image pixel is the electronic response of the input energy spectral distribution. Since flames are multi-wavelength sources of radiation (see Figure 1), by using hyperspectral devices or a multiple camera setup [8] it is possible to simultaneously record flame images at several waveband ranges. The disadvantages of these complex multispectral image devices, associated with their high cost, justifies the need to search for alternative systems with equivalent performance. Recently, some advances have been made to filter out significant data from color cameras for combustion diagnostics [9,10].

1.2. Our Contribution

In this paper, we propose to use the CCD color camera architecture as photo-sensors. We devise an optimized image processing methodology to diagnose the spatial distribution of burning conditions along the flame front, applied to laminar methane (CH_4) and propane (C_3H_8) gas premixed combustion, such as those of domestic appliances.
The remainder of this paper is organized as follows. Section 2 provides some background concepts and theory about image formation and the transfer function of the image acquisition process. Section 3 details our image processing approach for flame analysis. In section 4, we describe the experimental setup used in this work as well as some experimental results of our approach. Finally, section 5 ends the paper with some concluding remarks.

2. Background

2.1. Sensor Transfer Function

In digital color camera architecture, there are three types of sensor which correspond to the red (R), green (G), and blue (B) channels ($i \in \{R, G, B\}$). In fact, each sensor type corresponds to a waveband portion of the visible electromagnetic spectrum. To produce a color image, it is necessary to know at each pixel location the three channel values (r_R, r_G, r_B). In the typical 8 bit/pixel image representation, we have $r_i \in \{0, \ldots, 255\}$. Under a linear intensity-response model [11], a general form of the color camera response for a pixel of the i^{th} sensor type r_i, is given by

$$r_i = \varphi \kappa_i \frac{A\,\psi}{4\pi x^2} \Delta t \int_{\lambda_{min}}^{\lambda_{max}} S_i(\lambda)\, E(\lambda)\, d\lambda + \eta_i, \tag{1}$$

where $S_i(\lambda)$ is the overall system spectral sensitivity function of the type i sensor; $E(\lambda)$ is the flame spectral radiant flux per time unit; Δt is the exposure time and η_i is a normal random variable that corresponds to the *dark noise* of channel i. The integration limits λ_{min} and λ_{max} represent the wavelength boundaries of the photo-sensor sensitivity, outside which the system spectral response is negligible. Usually, for standard imagers, these limits cover all visible spectral range from around 370 nm to 720 nm (Figure 2). The camera model (1) also accounts for other sensor parameters such as camera gain (φ), channel gains (κ_i), pixel area (A), or focal distance (x). All geometric effects resulting from the f-number of camera aperture, observation angle, and lens anisotropy on light intensity signal can be described by a camera geometric coefficient ψ. In the present analysis, it was assumed that all these camera controls are invariant, so ψ can be considered roughly constant.
In fact, the camera image data corresponds to the light measured simultaneously by the three sensor types having distinct spectral sensitivity function $S_R(\lambda)$, $S_G(\lambda)$, and $S_B(\lambda)$ for the overall combination of lens/optics/sensors (Figure 2). These functions may be considered as three waveband responding separately to light emissions in distinct spectral regions. Thus, the signal detected by each of the camera sensor types is a complex function of the flame emission distribution $E(\lambda)$, filtered by the optical sensors over the quantum efficiencies $S_i(\lambda)$.

2.2. Energy Flux Analysis

The energy flux $E(\lambda)$, or the light emitted by the flame, results from two main contributions:

i) a non-linear dependence on equivalence ratio (through chemical kinetics) that reflects a different proportionality among chemiluminescent emitter species; and
ii) a linear dependence on power effect which tends to actuate on the entire spectrum, as a wideband controlling the emitted intensity.

Decomposing both effects, $E(\lambda)$ can be described by a specific distribution $E_\phi(\lambda)$, which encompasses wavelength dependent characteristics such as ϕ, and a scale factor function ω associated to non-wavelength dependent phenomena, given by $E(\lambda) = \omega\, E_\phi(\lambda)$. Considering

$$C_i(\phi) = \int_{\lambda_s}^{\lambda_f} S_i(\lambda)\, E_\phi(\lambda)\, d\lambda, \tag{2}$$

and defining a true camera photometric response r_i^* ($= r_i - \eta_i$), then (1) can be rewritten as

$$r_i^* \;=\; J_i\, C_i(\phi), \tag{3}$$

being

$$J_i \;=\; \varphi \kappa_i \frac{\omega A \psi}{4\pi x^2} \Delta t, \tag{4}$$

which, for a specific lens/optics/sensor configuration, is an exclusive function of the light intensity that reaches the sensor. Changes in scene luminance, image exposure time, camera gain or distance between sensor and image object,

induces proportional variations in the J_i values. Notice that adjustments on sensor gain κ_i produce distinct outcomes, since they yield an uneven effect on the pixel intensity level. Being J_i linearly dependent on intensity level I^*, defined by arbitrary combinations of weighted data from all sensor channels (r_R^*, r_G^*, r_B^*), the sensors intensity-response function (3) can be written as the semi-empirical relation

$$\frac{r_i^*}{I^*} = \tilde{k}_i(\phi), \tag{5}$$

where $\tilde{k}_i(\phi)$ is a combined function of lens/optics/sensors characteristics and flame response to ϕ, which is invariant with respect to the pixel intensity level I^*. The experimental acquisition of $\tilde{k}_i(\phi)$ data from flames at reference conditions, constitutes the sensor system calibration.

Table 1. Set of 12 descriptors used for flame image processing. The r_i^* generically denotes each of the three RGB components of the input color image, I.

♯	***Descriptor***	♯	***Descriptor***	♯	***Descriptor***	♯	***Descriptor***
1	r_R^*	4	$r_B^* \,/\, r_G^*$	7	$r_R^* \,/\, (r_R^*+r_G^*+r_B^*)$	10	$(r_R^*\times r_G^*) \,/\, r_B^*$
2	r_G^*	5	$r_G^* \,/\, r_R^*$	8	$r_G^* \,/\, (r_R^*+r_G^*+r_B^*)$	11	$(r_R^*\times r_B^*) \,/\, r_G^*$
3	r_B^*	6	$r_R^* \,/\, r_B^*$	9	$r_B^* \,/\, (r_R^*+r_G^*+r_B^*)$	12	$(r_B^*\times r_G^*) \,/\, r_R^*$

3. Proposed Approach

This section describes the proposed approach for flame image data analysis. input is an high resolution/ RGB color image (Figure 3) along with the flame reference parameters $\tilde{k}_i(\phi)$, to perform its analysis, according to a selected set of numerical relations (*descriptors*) and polynomial functions. The *descriptor* designation corresponds to simple numerical operations involving raw image data r_i^* (see Table 1). The method outputs an image representing the spatial distribution of flame equivalence ratio, computed as a weighted combination of a given number of descriptors. Algorithm 1 details the actions taken by our approach.

Line 6 of Algorithm 1 requires some explanation; the *getDescriptor*(F, $desc$) action returns the i^{th} image descriptor (a $M\times N$ gray-scale image) for the input RGB image F. The action *getPolynomial*($\mathcal{P}$, j), taken in line 8 of Algorithm 1, returns the j^{th} polynomial from the set of the input calibration polynomials $\tilde{k}_i(\phi)$. These polynomials were previously computed as functions of camera assembly, fuel type, and other sensor operative conditions.

Due to the large resolution of the color images, the number of descriptors and polynomials to evaluate, care must be taken in order to achieve reasonable running times, consistent with on-line sensing applications. Since after line 10 of Algorithm 1, many locations of the resulting matrices are zero, an approach using sparse matrices is devised. A sparse matrix has an efficient memory representation, since that it only stores the locations and values of the non-zero entries. Keeping the original (non-sparse) representation for the color images, in many cases a common *personal computer* (PC) may not have enough memory resources to store and process the data. On the other hand, even if there is enough storage memory, the running time will be prohibitive (several hours or even days), which would have as a consequence that the proposed technique may not be used as a sensing device. Thus, the *processDescriptor* action (line 14 of Algorithm 1) for each polynomial is carried out with sparse matrices, applying each descriptor, by an iterative process, for $j \in \{1, \ldots, P\}$, as follows:

- identify the location of pixels such that they are above and below the thresholds defined by $down_j$ and up_j;
- compute the average ϕ values on these locations and evaluate $poly_j$ on the entire grayscale image, F_g;
- the resulting matrices from the previous steps are multiplied.

The values from previous actions are combined, with a weighted sum based on normalized local derivatives, to produce the resulting image for each descriptor. The *processDescriptor* step returns two sparse matrices:

- the processed image, F_d, with all polynomials, for each descriptor $d \in \{1, \ldots, D\}$;

Algorithm 1 Equivalence Ratio Distribution Computation

Input: F, $M \times N$ RGB flame image;
D, number of image descriptors;
P, number of polynomials per descriptor;
$\mathcal{P}$, set of calibration reference polynomials;
Th_l, Th_h, lower and upper thresholds for descriptor comparison;
Output: F_w, $M \times N$ weighted image of flame equivalence ratio distribution;

1: Convert the RGB image F into the corresponding gray-scale image F_g. {/* Get both RGB and gray-scale images.*/}
2: Crop both F and F_g (see below and Figure 3) to isolate the flame area. Keep the results in F and F_g. Update M and N.
3: Apply a lower threshold operation on both F and F_g; all pixels below Th_l are set to 0.
4: Apply a upper threshold operation on both F and F_g; all pixels above Th_h are set to 255.
5: **for** $desc = 1$ to D **do**
6: $F_d = getDescriptor(F, desc)$. {/* Get corresponding image descriptor.*/}
7: **for** $j = 1$ to P **do**
8: $poly_j = getPolynomial(\mathcal{P}, j)$. {/* Get each polynomial from the set of calibration polynomials.*/}
9: $F_{dj} \leftarrow$ apply $poly_j$ on each pixel of F_d. {/* Evaluate each polynomial on each pixel.*/}
10: Apply a threshold operation on F_{dj}; all pixels below Th_l are set to 0; all pixels above Th_h are set to 255.
11: Compute $down_j \leftarrow$ the image locations where F_{dj} is below F_d. {/* Compare the image with the descriptor.*/}
12: Compute $up_j \leftarrow$ the image locations where F_{dj} is above F_d.
13: **end for**
14: $[F_d, M_d] \leftarrow processDescriptor(F_g, down_j, up_j, j, poly_j)$, with $j \in \{1, \ldots, P\}$. {/* Evaluate each descriptor.*/}
15: **end for**
16: Compute the weight mask from the binary masks $W[m,n] = \frac{1}{D} \sum_{d=1}^{D} M_d[m,n]$, with $m \in \{1, \ldots, M\}, n \in \{1, \ldots, N\}$.
17: Compute the final weighted flame image $F_w[m,n] = \sum_{d=1}^{D} W[m,n] F_d[m,n]$, with $m \in \{1, \ldots, M\}, n \in \{1, \ldots, N\}$.

- a binary mask image, M_d, with the same resolution holding the pixel locations of the active pixels, for each descriptor.

From the set of D matrices, with binary masks holding the location of the active pixels, M_d, with $d \in \{1, \ldots, D\}$, the final weight of each pixel, given by $W[m,n]$, is computed. This weight is the percentage of active descriptors, for each pixel (line 16 of Algorithm 1). Using $W[m,n]$, the resulting images from each descriptor are combined to compute the final weighted equivalence ratio distribution.
In order to speedup the image processing algorithm, a fully automatic (without human intervention) *crop procedure*, to isolate the flame image from the background, was proposed, as follows:

- convert the gray-scale F_g image to its binary version F_b, using Otsu's method [12];
- apply a median filter [13] with a mask of 25×25 pixels on F_b, to remove spurious pixels;
- find the rectangular *region of interest* (ROI) delimited by the pixels that remain at value 1;
- perform an image crop with the previously computed ROI.

The right-hand-side of Figure 3 shows the results of this procedure (referred in line 2 of Algorithm 1). Notice that it is able to automatically determine the flame position and to extract the relevant/informative portion of the image, yielding an image with fewer pixels to process, as compared to the original one.

4. Experimental Evaluation

This section briefly describes the experimental facilities and equipment used as well as some application results for the proposed image processing algorithm.

4.1. Combustion System

The burning assembly was formed by a circular Bunsen-type burner with an outlet diameter of 20 mm, used to produce laminar gas premixed flames taken as calibration references. High purity ($\geq$ 99.95%) methane (CH_4) and propane (C_3H_8) fuels supplied in gas cylinders were used and compressed atmospheric air as oxidizing. During experiments, fuel and air flows to the burner were measured by precision mass flow controllers (Alicat Scientific) having high accuracy corresponding to 0.4% of flow reading plus 0.2% of full scale. Experimental combustion conditions were tested at flame power of 0.75 to 1.75 kW, in a range of equivalence ratios between 0.80 and 1.40, having an estimated maximum error of $\pm$0.01 on the ϕ value.

4.2. Camera System

The imaging system used in this study is a RGB color 3-CCD area scan camera (JAI CV-M9GE) with a resolution of 1024(h)×768(v) active pixels per channel, 4.65 μm square cell size, 12 bit data depth, 30 frames/second at full resolution, and signal-to-noise ratio above 50 dB (on green). Optical lens was a ultraviolet/visible 105 mm CoastalOpt SLR lens, having light transmission efficiencies higher than 85% in the near-ultraviolet/visible range (250-650 nm).The steep spectral response curves (Figure 2) resulting from the dichroic prism coating reduce crosstalk between channels, being expected less color contamination and thus an enlargement of the pixel dynamic range. For flame image analysis. a fixed optical aperture $f/11$ was used and sensor exposure time varied from 1 ms up to 2 s. The acquired flame images were stored in raw format without further image processing nor color adjustment, and data extracted using the *MATrix LABoratory* Matlab platform running on a PC. Each color channel has the R, G, and B raw intensity value at full spectral resolution, and thus there is no need for image interpolation.

4.3. Calibration Data

Images of flames, at reference burning conditions, collected using the previously described camera system, were processed in order to compute the sensor $\tilde{k}_i(\phi)$ (line 8 of Algorithm 1), used as calibration data in the processing algorithm. After computing the ROI in the image, corresponding to the flame front, an average value of gray-scale

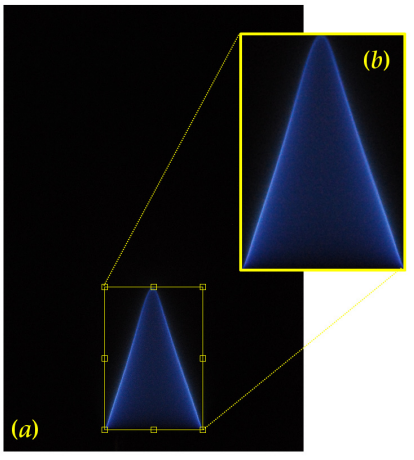

Fig. 3. The cropping procedure: (*a*) initial flame image; (*b*) cropped image. In this case, the cropping procedure reduces the number of pixels to around 12.4% of its initial value, maintaining image resolution.

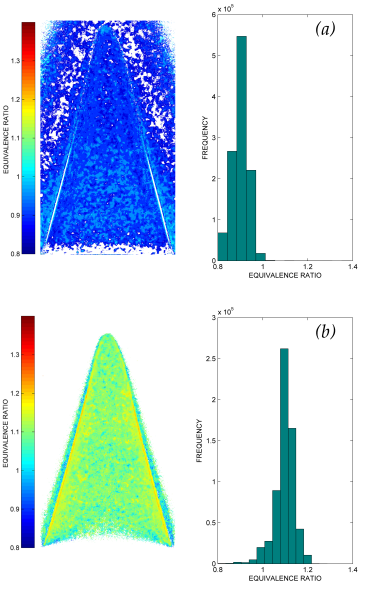

Fig. 4. Equivalence ratio images computed by Algorithm 1, according to three descriptors (#4, #8, and #11 of Table 1): (*a*) lean C_3H_8 flame at ϕ=0.90; and (*b*) rich CH_4 flame at ϕ=1.10. The bar graphs are the histograms of equivalence ratio frequency distribution.

intensity I^* and signal r_i^*, for each descriptor type, was extracted. The pairs (I^*, r_i^*) are characteristic of the flame equivalence ratio for the sensor system used. Extending the analysis to flame images obtained at different camera shutter speed, the overall range of pixel intensity I^* is covered and all possible combinations of r_i^* were produced. Extending further the analysis for images of flames at different ϕ, shutter speed and hydrocarbon gas fuel type, by processing the images according to all descriptors, a reference calibration table was build. This data was used to generate a set of polynomial coefficients to describe $\tilde{k}_i(\phi)$, thus yielding the sensor calibration.

4.4. Results and Discussion

An important aspect of our research is the evaluation of the possible use of standard CCD cameras and common processing equipment as bi-dimensional sensors of combustion conditions. The spatial sensing acuity is proportional to the image resolution, which in turn requires higher computational effort. Our algorithm running on a Matlab platform constitutes an appliance to assess that knowledge. Roughly, the total processing time can be assigned to four major generic computing steps: *memory management* (MM), *image cropping* (IC), *descriptor processing* (DP), and computing the *weighted output data* (WOD).

The MM step refers to the memory allocation and deallocation actions, required to build the necessary variables and data structures for image processing. The IC step in line 2 of Algorithm 1, discussed in section 3, applies some well-known image processing techniques, with efficient implementations, on the grayscale image version (which is faster than its use on the RGB version). The DP step applies a set of polynomial evaluations on *all* the pixels of the processed image. Finally, the WOD step, which includes the conversion from sparse to non-sparse (standard) matrix, is quite fast.

From the computational point of view, the DP step is the most time consuming (Figure 5), due to large number of computations per pixel. On a reference image processing situation with D=5 descriptors, the MM step takes around 10% of the time, the IC step takes 13%, the DP step takes 75%, and the WOD step takes about 2% of the total time. A higher number of descriptors processed per image tends to decrease the relative proportion of the cropping step, increasing all other three (Figure 5). Any improvement on the descriptor processing would be of great interest since it affects the most demanding tasks. The optimization level achieved by using sparse matrices was essential to reduce the global processing time of an image from several hours to a few minutes, with lower memory requirements.

Another important feature that significantly contributed to a fast and efficient behavior of the image sensor, is the automatic identification of the image area, holding the flame image (the cropping action). Considering the example illustrated by Figure 3, the crop action reduces the image to 12.4% of its original size. A proportional reduction in the image processing time was expected, although a further speedup was obtained, being the processing time for the 12 descriptors in the cropped image only around 9.8% of the time required for the original one. It was verified that the cropping effect has an average descriptor processing acceleration higher than 5× the number of pixels processed per

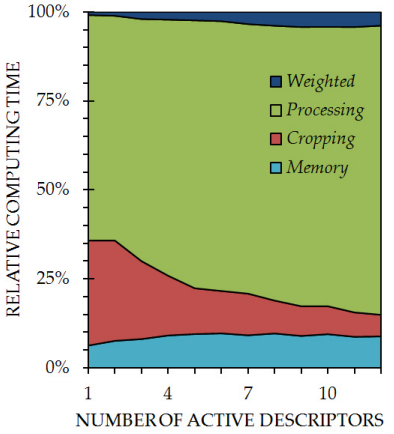

Fig. 5. Relative computation effort of Algorithm 1. Time distribution among the main code steps for a succession of descriptors processed.

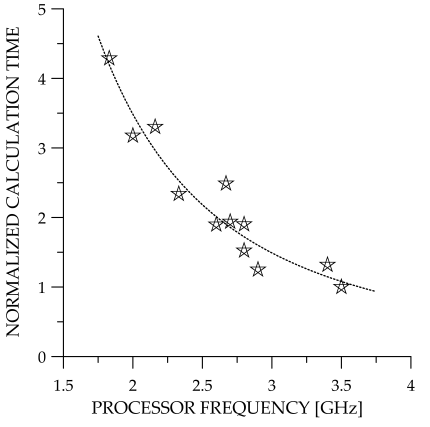

Fig. 6. Global time performances of Algorithm 1 on several computers characterized by their processor frequency. As normalization it was used the outcome of a 3.5 GHz PC.

second. This value tends to increase as the flame cropped area decreases being around 15× when the cropped image has only 5% of the initial image resolution. Therefore, this feature produces a two-way computing time reduction, *i)* due to the decrease in computed image size, and *ii)* due to the increase in the number of pixels processed per time unit.

With common equipment, the resulting performance does not yet yields a real time behavior. Taking a standard PC with 3.5 GHz of clock processor frequency, the average time required to process a single flame descriptor on a 1024(h)×768(v) image, is less than 2.3 s. As in the evaluation process of ϕ there is a need to use more than one descriptor, the image processing task induces a significant time delay on sensor response. A further generation of computing power is required to use this technology on fast control systems (Figure 6). However, other relevant uses like monitoring, diagnostics, quality control, among others, are some possible practical applications.

5. Conclusions

The use of sensors for proper evaluation of gas combustion systems is an important open problem, since it allows a suitable management of the combustion resources. It is presented here a contribution to improve performances of non-intrusive image sensors based on digital CCD technology. From high resolution images taken by an RGB color camera, it was devised an efficient image processing algorithm which is able to compute data in quasi real-time delivering the spatial distribution of flame equivalence ratio at the flame front. The approach, based on a restricted number of numerical descriptors, reference polynomials, sparse matrices, and (sparse) image processing operations is able to perform a flame image analysis in a few seconds on a standard personal computer. Practical combustion systems such as domestic water heating equipments, that uses laminar premixed methane/propane gas burners, have been analyzed by the sensor as a diagnostic and design improvement tool.

Acknowledgment

The authors want to acknowledge the technical and financial support of both: IN+ *Center for Innovation, Technology and Policy Research* and INScan Espectrometro gama Ultravioleta/Visivel/NIR (n. 21621) Projecto SI I&DT - Co Promoção - QREN.

References

[1] Kohse-Hoinghaus, K., Barlow, R., Alden, M., Wolfrum, J.. Combustion at the focus: laser diagnostics and control. Proceedings of the Combustion Institute 2005;30(1):89 – 123. doi:http://dx.doi.org/10.1016/j.proci.2004.08.274.

[2] Ballester, J., García-Armingol, T.. Diagnostic techniques for the monitoring and control of practical flames. Progress in Energy and Combustion Science 2010;36(4):375 – 411. doi:10.1016/j.pecs.2009.11.005.

[3] Hardalupas, Y., Orain, M., Panoutsos, C., Taylor, A., Olofsson, J., Seyfried, H., et al. Chemiluminescence sensor for local equivalence ratio of reacting mixtures of fuel and air (flameseek). Applied Thermal Engineering 2004;24(11-12):1619 – 1632. doi:10.1016/j.applthermaleng.2003.10.028.

[4] Jeong, Y., Jeon, C., Chang, Y.. Evaluation of the equivalence ratio of the reacting mixture using intensity ratio of chemiluminescence in laminar partially premixed ch4-air flames. Experimental Thermal and Fluid Science 2006;30(7):663–673.

[5] Muruganandam, T., Kim, B.H., Morrell, M., Nori, V., Patel, M., Romig, B., et al. Optical equivalence ratio sensors for gas turbine combustors. Proceedings of the Combustion Institute 2005;30(1):1601 – 1609.

[6] Tripathi, M., Krishnan, S., Srinivasan, K., Yueh, F., Singh, J.. Chemiluminescence-based multivariate sensing of local equivalence ratios in premixed atmospheric methane-air flames. Fuel 2012;93(0):684 – 691.

[7] Kojima, J., Ikeda, Y., Nakajima, T.. Basic aspects of oh(a), ch(a), and c2(d) chemiluminescence in the reaction zone of laminar methane/air premixed flames. Combustion and Flame 2005;140(1-2):34 – 45.

[8] Schefer, R.. Flame sheet imaging using ch chemiluminescence. Combustion Science and Technology 1997;126(1-6):255–279. doi:10.1080/00102209708935676.

[9] Huang, H.W., Zhang, Y.. Flame colour characterization in the visible and infrared spectrum using a digital camera and image processing. Measurement Science and Technology 2008;19(8):085406.

[10] Huang, H., Zhang, Y.. Digital colour image processing based measurement of premixed ch4 + air and c2h4 + air flame chemiluminescence. Fuel 2011;90(1):48 – 53. doi:10.1016/j.fuel.2010.07.050.

[11] Vora, P., Harville, M., Farrell, J., Tietz, J., Brainard, D.. Image capture: synthesis of sensor responses from multispectral images. Proceedings SPIE, Color Imaging: Device-Independent Color, Color Hard Copy, and Graphic Arts II 1997;3018:10. doi:10.1117/12.271577.

[12] Otsu, N.. A threshold selection method from gray-level histograms. IEEE Transactions on Systems, Man and Cybernetics 1979;9(1):62–66.

[13] Lim, J.. Two-dimensional Signal and Image Processing. Prentice Hall; 1990.